ACS OMEGA

http://pubs.acs.org/journal/acsodf

Article

Methylene Blue Removed from Aqueous Solution by Encapsulation of Bentonite Aerogel Beads with Cobalt Alginate

Yaohui Sun, Yanhui Li,* Bing Chen, Mingzhen Wang, Yang Zhang, Kewei Chen, Qiuju Du, Yuqi Wang, and Xinxin Pi

Cite This: *ACS Omega* 2022, 7, 41246−41255

Read Online

ACCESS | Metrics & More | Article Recommendations | Supporting Information

ABSTRACT: It can be difficult to remove dark methylene blue (MB) from water effectively. The use of sodium alginate and bentonite (Ben) as the matrix produced a displacement reaction that occurred in cobalt chloride, which allowed Ben to be successfully encapsulated in cobalt alginate (CA). Finally, a vacuum freeze-drying method was used to prepare a low-cost composite of CA/Ben aerogel for adsorbing MB in aqueous solutions. In addition to scanning electron microscopy, thermogravimetric analysis, and Fourier transform infrared spectroscopy, the composites were also characterized and analyzed. Different adsorption experiments were conducted in order to determine the effects of dosage, pH, adsorption time, and temperature on the adsorption performance of the adsorbent. According to the results of the experiment, the adsorption capacity of CA/Ben aerogel was 258.92 $mg \cdot g^{-1}$, and the pseudo-first-order kinetic model and Freundlich isotherm model can fully explain the adsorption process of MB on this aerogel. The composite material reported in this paper is easily recycled, and the removal rate reaches 65% after four times of recycling. Moreover, compared with other adsorbents, the composite material of the invention is highly environmentally friendly and has a simple preparation process. A large-scale application of this technology is the removal of dyes from water on a large scale.

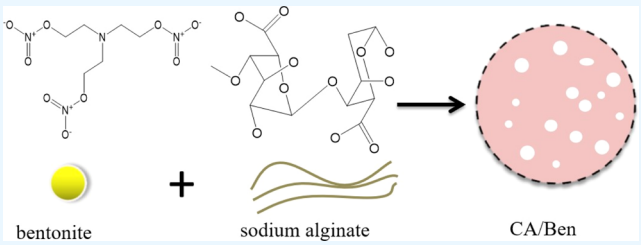

1. INTRODUCTION

During the past few years, with the continued growth of the printing and dyeing industry, dye pollution has become more serious, and the polluted water has caused serious health problems in humans.[1] Not only to dyes cause many life-threatening diseases in humans, but they also reduce the aesthetic value of water bodies. It is difficult to process most dyes due to their complex structure and deep color.[2] One of the most common cationic dyes is methylene blue (MB).[3] Due to its flat form, MB is easy to aggregate and highly soluble in solution, making it difficult to process.[4] Furthermore, exposure to MB can result in symptoms, such as nausea and breathing difficulties, and even a small micromolar concentration can cause harm to the human body.[5] A number of methods have been used to remove dyes from wastewater, including advanced oxidation processes,[6] aerobic or anaerobic digestion,[7] and coagulation.[8] There are, however, a number of disadvantages to these methods, including high costs, low efficiencies, and environmental effects.[9] In addition to developing green decolorization and decontamination methods, the industry also demands a cost-effective and sustainable solution.[10] In terms of wastewater treatment technologies, adsorption is considered as one of the most operational,[11] it is extremely popular in most developing countries, as it is able to meet most needs.[12,13]

Sodium alginate (SA) is a kind of natural polysaccharide, which has the characteristics of stability, safety, and non-toxicity.[14] Additionally, SA can be complexed with divalent metal cations (Ca^{2+}, Cu^{2+}, Co^{2+}, etc.) to form hydrogels.[15] It is commonly used as a thickener in order to increase the viscosity of the medium.[16] As a result, it is used in conjunction with other adsorbents in order to achieve the reusability of adsorbents. Graphene oxide (GO) has been reported to have excellent wastewater treatment properties due to its large surface area and a large number of functional groups.[17,18] Because GO has a high manufacturing cost and a complex preparation process, it is particularly important to find a material, which is as efficient and inexpensive as GO. Bentonite (Ben) is a layered clay mineral composed mainly of montmorillonite.[19] Ben has been widely used due to its high efficiency and low cost.[20] Previous studies have demonstrated that hydroxyl groups on the Ben surface are conducive to hydrogen bond formation and that these hydrogen bonds contribute to the improvement of the internal structure of the

Received: August 2, 2022
Accepted: October 26, 2022
Published: November 3, 2022

https://doi.org/10.1021/acsomega.2c04904
ACS Omega 2022, 7, 41246−41255

aerogel when combined with other polysaccharides.[21] Clay surfaces also have exchangeable ions, which leads to the clay through adsorption and ion exchange of negative and cation ions.[22] According to Errais et al., clay minerals remove dye from water at a rapid rate. Generally, natural clays are negatively charged and exhibit good adsorption properties for cationic dyes.[23] Unfortunately, if Ben is used directly for adsorption, sludge will be generated, causing re-pollution of the water body.[24] Due to its excellent performance in wastewater treatment, a large number of studies on Ben have been carried out by predecessors (such as calcium alginate/Ben composite,[25] cellulose/GO/Ben composite,[26] and Ben/activated carbon composite[16]). The use of alginate to encapsulate the Ben can effectively prevent the Ben from causing secondary pollution to the water body during the process of adsorbing dyes, and achieve the effect of reusability. In this paper, composite gel beads of different proportions of SA and Ben were formed by encapsulating Ben with SA. Then, the composite material was freeze-dried using a vacuum freeze dryer to synthesize cobalt alginate/bentonite (CA/Ben) aerogel composite material. Ben's high adsorption performance is retained in the composite, which results in the recovery of the adsorbent. As a consequence, the hydroxyl functional groups on the surface of Ben contribute to improving the internal structure of the aerogel when combined with polysaccharides.

The primary objective of this research is to synthesize low-cost and high-efficiency aerogel composites by encapsulating Ben via CA. The composites were characterized and analyzed using scanning electron microscopy (SEM), thermogravimetric analysis (TGA), and Fourier transform infrared spectroscopy (FTIR), and their ability to remove MB was described and evaluated.

2. MATERIALS AND METHODS

2.1. Material. SA was provided by Shanghai Aibi Chemical Co., Ltd., China. Xincheng Mineral Development Company (China) supplied the bentonite. Sulfuric acid (H_2SO_4, 98%), cobalt chloride hexahydrate ($CoCl_2{\cdot}6H_2O$), and hydrochloric acid (HCl, 36.0−38.0%), China Sinopharm Chemical Reagent Co., Ltd. Various other experimental reagents were obtained from China Aladdin Industrial Co., Ltd. The drugs were all of analytical grade and can be used directly without purification. The desired solution was prepared using deionized water.

2.2. Preparation of CA/Ben. To prepare the gel beads, 0.3 g SA was added to 30 mL of deionized water and stirred to dissolve it completely, then Ben was added to the beaker, and stirred continuously for 3 h. Under the stirring action of a magnetic stirrer, the mixed solution was injected into 5 wt % cobalt chloride solution with a syringe. The beads were washed several times with deionized water to remove residual cobalt chloride from the surface. After the gel beads were washed, they were frozen in the refrigerator overnight and then freeze-dried in a vacuum freeze-dryer. As can be seen in Figure 1, the optical contrast images before and after CA/Ben compounding clearly demonstrate the encapsulation of Ben by CA. To achieve the contrast effect, pure CA and Ben and CA and Ben with different mass ratios were prepared (CA/Ben = 0.1, 0.2, 0.3, 0.4).

2.3. Material Characterization. SEM was used to examine the morphological characteristics of CA/Ben. A thin layer of gold powder was sprayed on the sample's surface before analysis, and the measurement was conducted at a voltage of 20 kV. TGA under a nitrogen atmosphere at a heating rate of 10 K·min^{-1} was used to investigate the thermal stability of CA/Ben composites. Under vacuum at 423 K, the sample material was dried for 5 h. An automatic surface analyzer is used to determine pore size distribution and Brunauer−Emmett−Teller (BET) area at 77 K based on the N_2 adsorption and desorption isotherm. In order to prepare 0.01 M NaCl solution, 10 mg of sorbent was added to 20 mL of sodium chloride solution and the pH accordingly was adjusted. In order to explain the effect of pH on the adsorption performance of the adsorbent (pH values using different concentrations of HNO_3 and NaOH solutions was adjusted). Zeta points were used to measure the charge properties of the material surface.

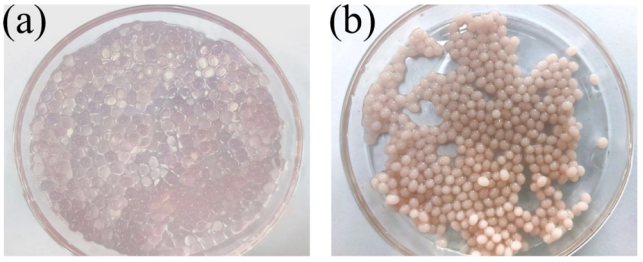

Figure 1. Optical contrast images before and after CA/Ben compounding: before compounding (a) and after compounding (b).

2.4. Adsorption Experiments. In deionized water, MB in deionized water was dissolved to prepare the original solutions (1000 mg·L^{-1}) of the desired dye concentrations. A fixed weight (10 mg) of CA/Ben was added to a 50 mL Erlenmeyer flask containing 20 mL of MB solution (40−140 mg·L^{-1}). MB solutions of 100 mg/L were used to determine the adsorption properties of composites with different weight ratios. Adsorption equilibrium was reached after 48 h of shaking the solution. In order to measure the remaining dye concentration in the solution after centrifugation, a UV−vis spectrometer (TU-1810, Beijing Pujinye General Instrument Co., Ltd., China) was used. A 120 rpm air-bath shaker was used for all adsorption experiments, while all other conditions remained unchanged. The adsorption equilibrium capacity (q_e, mg·g^{-1}) and removal rate (D, %) were calculated using the following formulas.

$$q_e = \left(\frac{C_0 - C_e}{m} \times V\right) \quad (1)$$

$$D\,\% = \left(\frac{C_0 - C_t}{C_0}\right) \times 100 \quad (2)$$

where, C_0, C_e, and C_t (mg·L^{-1}) represent the initial concentration of dye, the concentration of dye after equilibrium, and the concentration of dye at time t respectively; and V and m are the dye volume (mL) and adsorbent mass (mg), respectively.

3. RESULTS AND DISCUSSION

3.1. Material Characterization. SEM was used to examine the surface morphology of CA, Ben, and CA/Ben. According to Figure 2a, CA has a relatively dense and smooth surface, so it serves as a skeleton in this study. Ben has a relatively rough surface, as shown in Figure 2b, which explains its high dye adsorption capacity. At different magnifications, Figures 2c,d illustrates the surface morphologies of CA/Ben

https://doi.org/10.1021/acsomega.2c04904
ACS Omega 2022, 7, 41246−41255

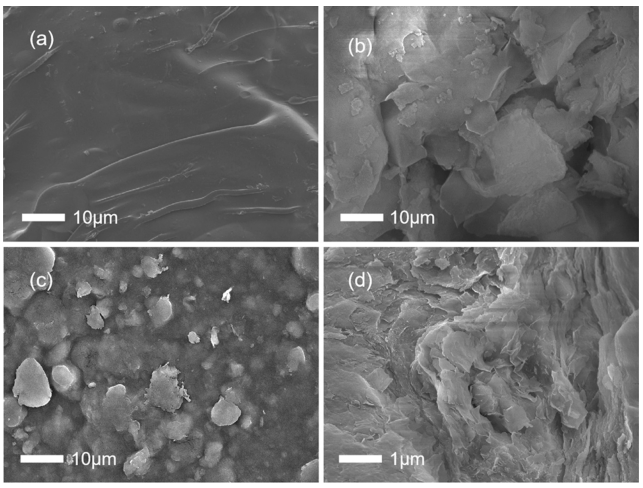

Figure 2. SEM images of CA (a), Ben (b), and CA/Ben at different multiples (c,d).

aerogels. From Figure 2c, it can be seen that there are more protrusions on the surface of CA/Ben, which indicates that Ben is encapsulated within CA. Moreover, the wrinkling of the material in Figure 2d is observed to increase significantly, further verifying that the addition of Ben improved the morphology and adsorption performance of CA.

As shown in Figure 3a, the TGA curves of CA, Ben, and CA/Ben composites can be viewed. Before 200 °C, all the samples in Figure 3a lost a significant amount of weight, mainly due to dehydration.[27] The weight losses of CA, Ben, and CA/Ben were 12.7, 10.5, and 6.1%, respectively. Between 200 and 600 °C, cobalt alginate and its composites exhibit noticeable mass loss, primarily as a result of the release of water with a closer polar interaction between carboxylate groups and the decomposition of oxygen-containing functional groups on the surface of cobalt alginate.[28,29] At 600 °C, each curve begins to decline slowly, which is largely due to the dehydroxylation reaction of aluminosilicate.[30] The enhanced cross-linking structure of the composite and the barrier effect of Ben result in a significant improvement in thermal stability. Additionally, it has been observed that the loss of Ben encapsulated in cobalt alginate is significantly greater than that of pure Ben, primarily due to the decomposition of alginate. Despite this, the thermal stability of CA/Ben is much better than that of pure CA, mainly due to the enhanced cross-linking structure and barrier effect of Ben. By using a TGA analyzer at 800 °C, CA, Ben, and CA/Ben lost 72.24, 17.07, and 47.43% of their weight, respectively.

As shown in Figure 3b, the functional groups of the composite CA/Ben and the combined component (CA, Ben) were characterized using FTIR spectroscopy. At 1640 and 1580 cm^{-1}, cobalt alginate exhibits vibrations related to the stretching of C═C double bonds and the vibrations related to the benzene ring skeleton.[31,32] The peaks at 1014 and 1400 cm^{-1} may be C−H in-plane bending vibrations and symmetrical stretching motions of carboxylate ions, respectively.[33,34] At 912 cm^{-1}, it may be a group composed of Al−Al−OH.[35] The characteristic peaks at 791, 623, and 520 cm^{-1} indicate bending vibration along the C−H chain, stretching vibration along the C−Cl chain, and bending vibrations along the Si−O chain, respectively.[36,37] Through the characterization of the material by FTIR spectroscopy, it can be seen that Ben was successfully encapsulated into CA, forming a new type of composite material. By comparing the FTIR representation of the adsorbent before and after adsorption in Figure 3b, it can be clearly seen that the peak value disappears at 1400 and 791 cm^{-1}. The carboxylic acid anion and hydrocarbon on the adsorbent may be involved in the adsorption reaction.

The BET specific surface areas of the composites CA/Ben and the constituents were determined by N_2 adsorption and

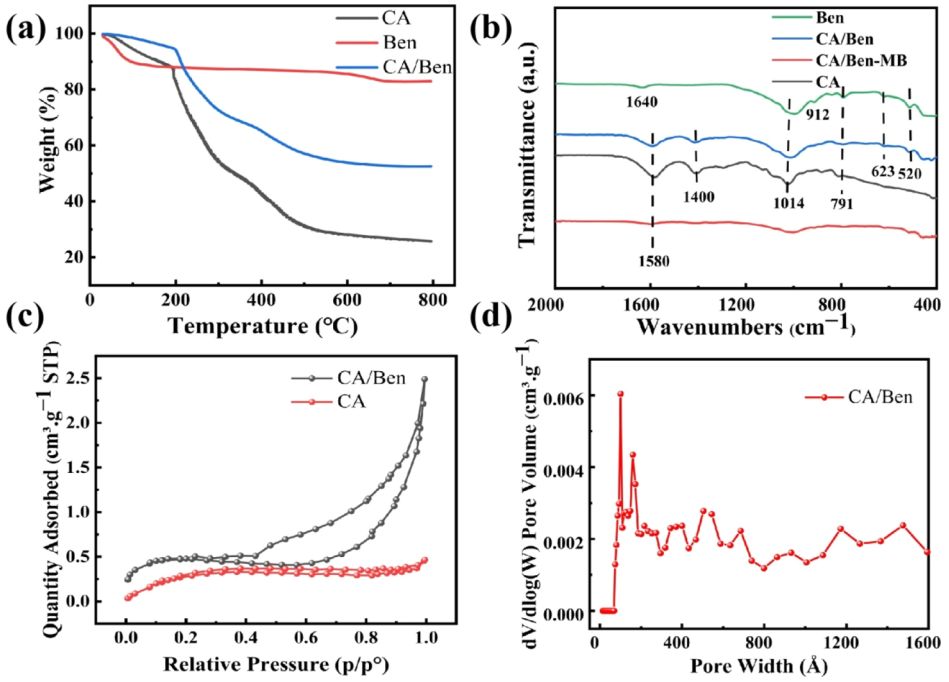

Figure 3. TGA curve (a) and FTIR curve (b) of different materials; N_2 adsorption−desorption curves (c) of CA and CA/Ben composites; and pore size distribution of CA/Ben composites (d).

https://doi.org/10.1021/acsomega.2c04904
ACS Omega 2022, 7, 41246−41255

desorption isotherms. As can be seen in Figure 3c, the curve type of CA conforms to the type II isotherm, which reflects the typical physical adsorption process on non-porous or macroporous adsorbents.[16] In addition, the BET specific surface area of CA is relatively small, which is 1.924 $m^2 \cdot g^{-1}$. The curve type of CA/Ben exhibits a compound IV isotherm curve type. This type of isotherm corresponds to a system in which the porous adsorbent exhibits capillary condensation, which is consistent with the H3 hysteresis loop, which indicating that the pore structure is very irregular. Due to the addition of Ben (58.7047 $m^2 \cdot g^{-1}$, as shown in Figure S1) to CA, the specific surface area of the obtained composite CA/Ben was increased (4.4628 $m^2 \cdot g^{-1}$). Figure 3d shows the pore size distribution curve of CA/Ben composites. The average adsorption pore size of the CA/Ben composite is 101.867 Å. According to the IUPAC pore size distribution, the composite was confirmed to be a mesoporous material.[38] According to previous studies, the molecular size of MB is 13.32 Å. Therefore, the composite CA/Ben can effectively adsorb and remove MB.[39]

3.2. Effects of Different Mass Ratios on Adsorption Performance. The optimal mass ratio can achieve the lowest cost and the highest benefit, so it is very important to explore the optimal mass ratio. In the experiments were carried out using the MB solution at a concentration of 100 $mg \cdot mL^{-1}$. Figure 4 shows that the MB removal rates of CA and Ben at

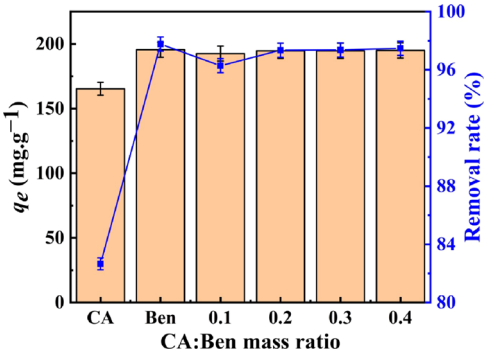

Figure 4. Effects of different mass ratios on the adsorption performance of CA/Ben.

different mass ratios (CA, Ben, CA/Ben = 0.1, 0.2, 0.3, 0.4) were 82.64, 97.77, 96.28, 97.35, 97.36, and 97.48%, respectively. Although Ben has a high removal rate, direct use will cause secondary pollution to the environment and cannot be recycled. For the composite materials with different mass ratios, the removal rate increases gradually with the increase of the ratio. The possible reason is that the combination of Ben and CA can improve the steric structure inside the alginate, thereby increasing the adsorption capacity. However, the mass of the added adsorbent is fixed, and the mass of Ben is heavier, so the smaller the proportion of Ben, the higher the removal efficiency. When CA: Ben = 0.2, with the increase of mass ratio, the removal rate does not change much. Considering the cost, the best mass ratio is CA: Ben = 0.2.

3.3. Effects of Dosage, pH, Time, and Temperature on Adsorption Performance. It is essential to determine the optimal amount of input adsorbent in order to maximize the benefits. Figure 5a depicts that, the removal rate of CA/Ben composites increased with the increase of adding amount from 92.34 to 99.60%, but the adsorption amount decreased gradually. The main reason for the increase of removal rate is that the removal rate of MB is positively proportional to the adsorption site on the surface of the adsorbent. Thus, with the increase of adsorption dose, adsorption sites also gradually increased. The main reason for the decrease of adsorption capacity is that although the adsorption sites gradually increase, the MB molecules are limited, which leads to the failure to maximize the utilization of active sites on the adsorbent surface.

The initial pH has a great influence on the adsorption of MB by adsorbent. Therefore, it is of great significance to explore the optimal pH value. The temperature chosen for this work was 298 K and 20 mL of MB solution at a concentration of 100 $mg \cdot L^{-1}$ was used for the experiment. This experiment investigated the effect of pH on the adsorbent and Zeta potential. As can be seen in Figure 5b, CA/Ben has zero charge site (pHpzc) at pH 5. This indicates that in pH < 5, the CA/Ben surface is positively charged. Electrostatic repulsion between the positively charged adsorbent and the cation is not conducive to the adsorption of the cation. The zeta point gradually decreased with the increase of pH. When pH > 5, the degree of deprotonation of −COOH and −OH groups increased, which was conducive to the removal of cationic dyes.[40] It can be found that in the range of pH 2−7, the removal rate increases with the increase of pH. It is possible that the zeta potential value of CA/Ben decreases, which reduces the effect of charge mutual exclusion. On the contrary, the removal rate of CA/Ben decreased with the increase of pH in the range of 7−10. At lower pH, the CA/Ben surface may become positively charged, which allows H^+ in solution to compete with cationic dyes.[41] The original pH value of MB solution is 7.37, and the removal effect of the composite material is the best when the pH value is 7, so the composite material is suitable for treating MB in most water bodies.[42] Because MB contains chloride ions, chloride ions may undergo a displacement reaction with NaOH in solution at higher pH values to generate NaCl (aq) and MBS^+OH (aq). Meanwhile, NaCl may reduce the adsorption of MBS^+OH by CA/Ben, thus reducing the removal rate of MB by CA/Ben.[43,44]

Temperature has an important effect on the adsorption rate and capacity of MB. Therefore, 10 mg of sorbent was added to 20 mL of MB solutions of different concentrations (40−140 $mg \cdot mL^{-1}$) and divided into the same three groups. This experiment examined the effects of different temperatures (298, 308, and 318 K) on adsorption properties of CA/Ben composites under the assumption that other conditions remained the same. Figure 5c shows the adsorption capacity of CA/Ben for MB at different temperatures. The maximum adsorption capacity of CA/Ben composite was 254.36 $mg \cdot g^{-1}$ at 298 K, and the adsorption capacity decreased to 247.05 $mg \cdot g^{-1}$ with the increase of temperature. The may be caused by weakened attraction between MB and adsorbent sites. The experimental results show that the adsorption process of the CA/Ben composite is an exothermic reaction. This is consistent with previous experimental results.[45]

Figure 5d depicts the adsorption rate of CA/Ben composite. The adsorption rate was fast within 160 min, and then the adsorption rate was slow until it reached equilibrium. The adsorption of MB by CA/Ben reached equilibrium after 1440 min. Table 1 shows the comparison of the adsorption rates of MB by various adsorbents. At the beginning, the adsorption rate was fast mainly because there were many adsorption sites in the initial stage, but as time went by, more and more

https://doi.org/10.1021/acsomega.2c04904
ACS Omega 2022, 7, 41246−41255

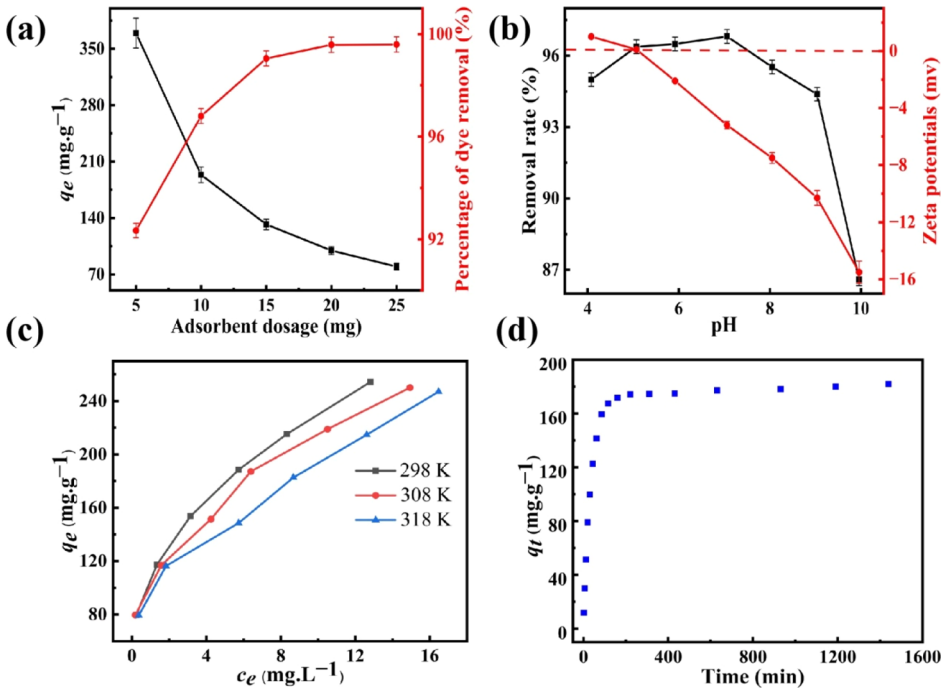

Figure 5. Effects of different experimental conditions on the adsorption of MB on CA/Ben: adsorbent dosage (a), pH (b), temperature (c), and time (d).

Table 1. Comparison of MB Adsorption Rate with Different Adsorbents

adsorbents	model of kinetic	balance time (h)	removal rate (%)	T (K)	refs
wet-torrefied microalgal biochar	pseudo-first-order	120	85	303	47
Alg/Ben	pseudo-second-order	33	60	298	25
NTA-β-CD-CS	pseudo-second-order	1.5	96	298	40
CS/SA fibrous foams	pseudo-second-order	20	95	298	48
CA/Ben	pseudo-first-order	24	97	298	this work

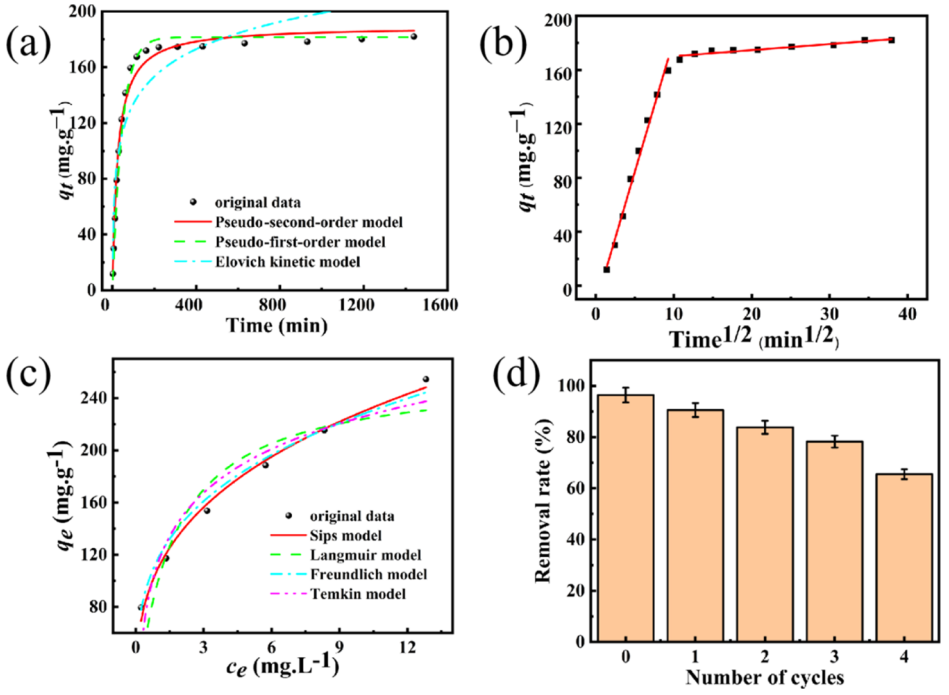

Figure 6. Adsorption kinetic model fitting (a); intraparticle diffusion model (b); adsorption isotherm fitting (c); and regeneration performance (d).

https://doi.org/10.1021/acsomega.2c04904
ACS Omega 2022, 7, 41246−41255

adsorption sites were occupied by MB molecules. The dye then diffuses into the adsorbent until it reaches equilibrium, resulting in a slower adsorption rate.[46]

3.4. Adsorption Kinetics. To better analyze the adsorption process, the experimental data were fitted with a Pseudo-first-order model, a Pseudo-second-order model, an Elovich kinetic model (Figure 6a), and an intraparticle diffusion model.[49−51] Where q_t and q_e in the formula represent the adsorption capacity at time t and the adsorption capacity after reaching the adsorption equilibrium, respectively. The pseudo-first-order model (eq 3), the pseudo-second-order model (eq 4), and Elovich kinetic model (eq 5) are formulated as follows

$$q_t = q_e(1 - e^{-kt}) \tag{3}$$

$$q_t = \frac{q_e v_0 t}{q_e + v_0 t} \tag{4}$$

$$q_t = \frac{\ln(\alpha\beta)}{\beta} + \frac{\ln(t)}{\beta} \tag{5}$$

where k (min^{-1}) refers to the rate constant of the pseudo-first-order model, v_0 ($mg{\cdot}g^{-1}{\cdot}min^{-1}$) refers to the adsorption rate when adding adsorbents. α ($mg{\cdot}g^{-1}{\cdot}min^{-1}$) and β ($g{\cdot}mg^{-1}$) are the initial adsorption rates and the parameters related to chemisorption activation energy and surface coverage extent, respectively.

The pseudo-first-order model is one of the most commonly used models, mainly used in the adsorption process in the liquid phase, indicating that the adsorption process is mainly affected by physical effects. For the adsorption conforming to the pseudo-second-order model, it can be considered that the adsorption process is affected by chemical action and not affected by physical migration. The Elovich model is mainly used to describe the adsorption behavior of pollutants on the non-uniform solid surface during the adsorption process.[32] The adsorption kinetic parameters and correlation coefficients are shown in Table 2, and the fitting curve of the adsorption process is more in line with the pseudo-first-order model (R^2 = 0.997).

The adsorption rate is mainly affected by membrane diffusion and particle diffusion.[52] According to the diffusion model, the adsorption process is divided into two parts. The intraparticle diffusion model formula is as follows

$$q_t = k_i t^{1/2} + c_i \tag{6}$$

where k_i ($mg{\cdot}g^{-1}{\cdot}min^{-1/2}$) is the constant with respect to the intraparticle diffusion rate and C_i ($mg{\cdot}g^{-1}$) is the intercept associated with the adsorption step.

The diffusion model was obtained by linear fitting (Figure 6b). The model was divided into two parts. The first stage is the rapid adsorption stage, which is mainly affected by membrane diffusion. At this stage, MB is rapidly adsorbed by the active site on the surface of the adsorbent. The second part is the intramolecular diffusion stage, where the adsorption rate is relatively slow, mainly the particle diffusion stage. Because both line segments do not pass through the origin, both membrane diffusion and intraparticle diffusion have an effect on the adsorption rate during the adsorption of MB by CA/Ben.[53]

3.5. Adsorption Isotherm. In this paper, Langmuir, Freundlich, Sips, and Temkin isotherm models were used to perform nonlinear fitting to the data of this study at 298 K, and the fitting results are shown in Figure 6c. Meanwhile, Table 3 describes the parameters of the nonlinear fitting of the Langmuir isotherm (eq 7), the Freundlich isotherm (eq 8), the Sips isotherm model (eq 9), and Temkin isotherm model (eq 10).

$$q_e = \frac{q_m K_L c_e}{1 + K_L c_e} \tag{7}$$

$$q_e = k_f c_e^{1/n} \tag{8}$$

$$q_e = \frac{q_m (K_s c_e)^b}{1 + (K_s c_e)^b} \tag{9}$$

$$q_e = B_T \ln(A_T c_e) \tag{10}$$

where K_L is a constant related to the strength of adsorption between the adsorption site and the adsorbent. K_f ($mg^{1-1/n}{\cdot}L^{1/n}{\cdot}g^{-1}$) is the constant used in the calculation, and n represents the degree of irregularity of the adsorbent surface. K_S [$(L{\cdot}mg^{-1})^{1/b}$] represents the parameters in the Sips model; b means the heterogeneity constant of Sips; and B_T ($J{\cdot}mol^{-1}$) describes the energy constant in the Temkin isotherm model, while A_T ($L{\cdot}mg^{-1}$) represents the equilibrium binding constant.

The Langmuir isotherm model assumes that the adsorption of dyes occurs on the adsorbent with limited and surface-homogeneous adsorption sites.[54] In contrast, the Freundlich isotherm model assumes that the adsorption process occurs on

Table 2. Fitting Results of Kinetic Model Parameters of MB Adsorption on CA/Ben

kinetic model	parameter	values
pseudo-first-order kinetic model	k (min^{-1})	0.027
	q_e($mg{\cdot}g^{-1}$)	176.523
	R^2	0.997
pseudo-second-order kinetic model	v_0($mg{\cdot}g^{-1}{\cdot}min^{-1}$)	7.648
	q_e($mg{\cdot}g^{-1}$)	189.426
	R^2	0.986
	α ($mg{\cdot}g^{-1}{\cdot}min^{-1}$)	31.920
Elovich kinetic model	β ($g{\cdot}mg^{-1}$)	0.033
	R^2	0.880
intraparticle diffusion model	k_1($mg{\cdot}g^{-1}{\cdot}min^{-1/2}$)	19.586
	C_1	−13.520
	R^2	0.989
	K_2($mg{\cdot}g^{-1}{\cdot}min^{-1/2}$)	0.452
	C_2	165.572
	R^2	0.905

Table 3. Model Parameters of Adsorption Isotherm of MB Adsorption by CA/Ben

models	parameters			
Langmuir	q_m($mg{\cdot}g^{-1}$) 258.919	K_L($L{\cdot}mg^{-1}$) 0.626		R^2 0.844
Freundlich	K_f($mg^{1-1/n}{\cdot}L^{1/n}{\cdot}g^{-1}$) 110.059	n 3.134		R^2 0.991
Sips	q_m($mg{\cdot}g^{-1}$) 274.096	K_s($L{\cdot}mg^{-1}$)$^{1/b}$ 0.569	b 0.324	R^2 0.990
Temkin	B_T($J{\cdot}mol^{-1}$) 48.183	A_T($L{\cdot}mg^{-1}$) 10.773		R^2 0.980

https://doi.org/10.1021/acsomega.2c04904
ACS Omega 2022, 7, 41246−41255

a multi-layered heterogeneous adsorbent surface.[55] Sips isotherm model is an improved formula of Langmuir and Freundlich model.[56] The Temkin isotherm model is used to describe the relationship between the adsorbent and the heat of adsorption.[57] It can be seen from Table 3 that the CA/Ben composites are more in line with the Freundlich isotherm model (R^2 = 0.991), which indicates that the adsorption of MB on CA/Ben aerogels is a multilayer heterogeneous surface adsorption. This assessment is consistent with that of the previous analysis. At the same time, the parameter n in the Freundlich isotherm model is between 2 and 10, indicating that the adsorption reaction is relatively easy to carry out. The maximum adsorption capacity of the adsorbent CA/Ben calculated by the Langmuir model was 258.919 mg·g^{-1}.

Different adsorbents were compared to find their advantages and disadvantages. Therefore, different adsorbents were found under similar conditions to conduct comparative experiments with CA/Ben. The comparison results are shown in Table 4. It can be seen that the adsorption performance of CA/Ben composites for MB is relatively excellent.

Table 4. Comparison of MB Adsorption Performance between CA/Ben and Other Adsorbents

adsorbents	dosage (mg·mL^{-1})	c_0 (mg·mL^{-1})	q_m (mg·g^{-1})	refs
ANaBC	1	10−800	201	58
plasma treated bentonite	0.75	100−250	303	59
CMC/KC/AMMT	0.1	10−500	12.5	60
PVA/PCMC/GO/Ben	1.5	50−250	172.4	26
CA/Ben	0.5	40−140	258.9	this work

3.6. Thermodynamic Studies. The adsorption of MB on CA/Ben can be further investigated by utilizing the Gibbs free energy change (eq 11) and calculating the thermodynamic parameters of the adsorption process (eq 12). where R is the universal gas constant (8.314 J·mol^{-1}·K^{-1}). ΔG, ΔH, and ΔS represent Gibbs free energy change, enthalpy change, and entropy change, respectively. The values of ΔH and ΔS can be obtained directly from the linear fit of $\ln(q_e/c_e)$ to $1/T$.

$$\Delta G = \Delta H - T\Delta S \tag{11}$$

$$\ln\left(\frac{q_e}{c_e}\right) = -\frac{\Delta H}{RT} + \frac{\Delta S}{R} \tag{12}$$

It can be seen from Table 5 that the Gibbs free energy is negative at all temperatures ($\Delta G \leq 0$). Meanwhile, the absolute value of ΔG decreases with increasing temperature, which indicates that the adsorption process is spontaneous and suppressed at high temperatures. In addition, $\Delta H \leq 0$, indicating that the adsorption process of MB on CA/Ben is an exothermic process.[61]

Table 5. Thermodynamic Parameters of MB Adsorption by CA/Ben

T (K)	ΔG(kJ·mol^{-1})	ΔH(kJ·mol^{-1})	ΔS(J·mol^{-1} K^{-1})
298	−11.072	−12.511	−4.830
308	−11.023		
318	−10.975		

3.7. Recycling Performance. The re-recovery performance is one of the important criteria for evaluating the practical value of the adsorbent, and its performance determines the cost of using the adsorbent. In order to evaluate the re-recycling performance of CA/Ben composites, MB solution with a concentration of 100 mL was carried out at 25 °C under natural pH conditions. Due to certain mass loss during the re-recovery process, the ratio of adsorbent to dye was kept constant at 1:2 in each re-recovery experiment. After adsorption, 0.1 M hydrochloric acid solution was used for desorption and after complete desorption, deionized water was used for several times to wash off excess hydrochloric acid solution. The samples were vacuum freeze-dried and then adsorbed again. The above process was repeated 4 times, and the experimental results are shown in Figure 6d. The dye removal rate decreased from 97.38 to 65%, possibly because the Co−O bond might break in the acidic solution. After the fifth repeated adsorption, the morphology of the composite will be destroyed. At the same time, the decrease of adsorption capacity may also be due to the adsorption site is still partially occupied during each desorption process, and the desorption is not complete.

3.8. Adsorption Mechanism. Figure 7 shows the adsorption mechanism diagram of MB adsorbed by CA/Ben. The adsorption process of dyes is usually closely related to electrostatic attraction, hydrogen bonding, and $\pi-\pi$ interactions.[62] According to previous studies, the oxygen-containing functional groups on the surface of cobalt alginate can interact with cationic dyes. Because Ben itself has strong ion conversion ability, the addition of Ben improves the adsorption efficiency. In order to better understand the adsorption mechanism, the FTIR spectrum of the sample (CA/Ben-MB) after adsorption of MB was recorded, as shown in Figure 3b. The characteristic peak of MB at 1587 cm^{-1} appears on the spectrum.[63] At the same time, the intensity of carboxylate functional groups in CA/Ben was observed to change, which confirmed that MB was adsorbed to the composite active site. In addition, with the increase of pH, the hydroxyl and carboxyl groups in the cobalt alginate composites were deprotonated to form O^- and COO^- groups, which improved the electrostatic attraction properties of the CA/Ben composites to MB.[64]

4. CONCLUSIONS

In this paper, inexpensive and efficient composite aerogel beads (CA/Ben) based on cobalt alginate and bentonite were successfully synthesized. It was confirmed that Ben was indeed encapsulated in CA by observation of optical pictures and FTIR spectroscopic analysis. By exploring different mass ratios and the conditions affecting the adsorption performance, the optimal mass ratio and adsorption conditions were obtained (CA: Ben = 0.2, 298 K, pH 7, adsorbent mass 10 mg). The introduction of Ben did enhance the adsorption capacity of the aerogel for MB. Through a series of characterization analysis (SEM, TGA, and BET) of CA/Ben, it was found that the addition of Ben promoted the formation of rough structure, thermal stability, and specific surface area of the aerogel surface. The adsorption of MB on CA/Ben can be well described by pseudo-first-order kinetic model and Freundlich isotherm model. The prepared aerogel can maintain a high removal rate after four adsorption−desorption cycle experiments, so the prepared composite material can be used as an efficient and environmentally friendly adsorbent in the field of dye treatment.

https://doi.org/10.1021/acsomega.2c04904
ACS Omega 2022, 7, 41246−41255

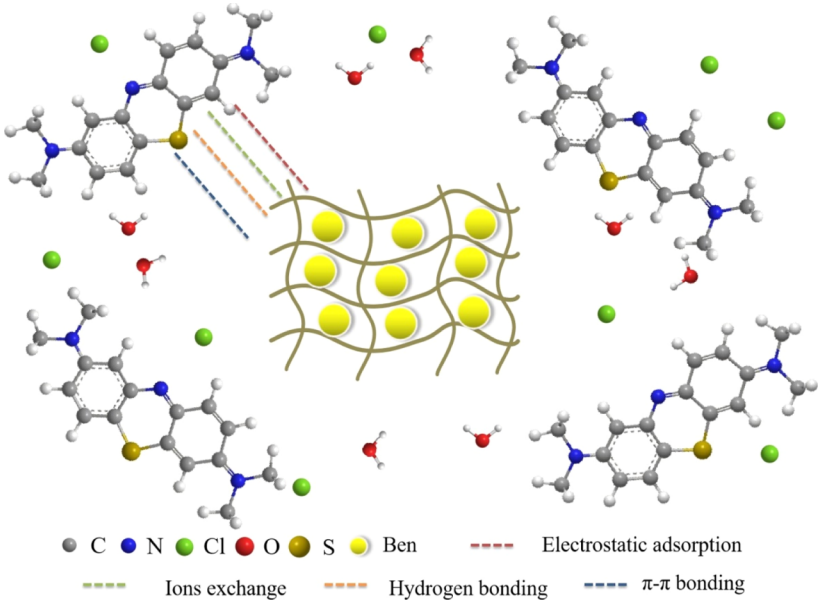

Figure 7. Adsorption schematic diagram.

■ ASSOCIATED CONTENT

Supporting Information

The Supporting Information is available free of charge at https://pubs.acs.org/doi/10.1021/acsomega.2c04904.

Ben's N_2 adsorption and desorption curve (PDF)

■ AUTHOR INFORMATION

Corresponding Author

Yanhui Li − *College of Mechanical and Electrical Engineering, Qingdao University, Qingdao 266071, China; State Key Laboratory of Bio-fibers and Eco-textiles, College of Mechanical and Electrical Engineering, Qingdao University, Qingdao 266071, China;* orcid.org/0000-0001-7370-0233; Email: liyanhui537@163.com

Authors

Yaohui Sun − *College of Mechanical and Electrical Engineering, Qingdao University, Qingdao 266071, China*

Bing Chen − *College of Mechanical and Electrical Engineering, Qingdao University, Qingdao 266071, China*

Mingzhen Wang − *College of Mechanical and Electrical Engineering, Qingdao University, Qingdao 266071, China*

Yang Zhang − *College of Mechanical and Electrical Engineering, Qingdao University, Qingdao 266071, China*

Kewei Chen − *College of Mechanical and Electrical Engineering, Qingdao University, Qingdao 266071, China*

Qiuju Du − *State Key Laboratory of Bio-fibers and Eco-textiles, College of Mechanical and Electrical Engineering, Qingdao University, Qingdao 266071, China*

Yuqi Wang − *College of Mechanical and Electrical Engineering, Qingdao University, Qingdao 266071, China*

Xinxin Pi − *College of Mechanical and Electrical Engineering, Qingdao University, Qingdao 266071, China*

Complete contact information is available at: https://pubs.acs.org/10.1021/acsomega.2c04904

Notes

The authors declare no competing financial interest.

■ ACKNOWLEDGMENTS

The authors are grateful to the National Natural Science Foundation of China (51672140) and Taishan Scholar Project of Shandong Province (201511029).

■ REFERENCES

(1) Yang, M.; Liu, X.; Qi, Y.; Sun, W.; Men, Y. Preparation of kappa-carrageenan/graphene oxide gel beads and their efficient adsorption for methylene blue. *J. Colloid Interface Sci.* **2017**, *506*, 669−677.

(2) Xing, R.; Wang, W.; Jiao, T.; Ma, K.; Zhang, Q.; Hong, W.; Qiu, H.; Zhou, J.; Zhang, L.; Peng, Q. Bioinspired Polydopamine Sheathed Nanofibers Containing Carboxylate Graphene Oxide Nanosheet for High-Efficient Dyes Scavenger. *ACS Sustainable Chem. Eng.* **2017**, *5*, 4948−4956.

(3) Saya, L.; Gautam, D.; Malik, V.; Singh, W. R.; Hooda, S. Natural Polysaccharide Based Graphene Oxide Nanocomposites for Removal of Dyes from Wastewater: A Review. *J. Chem. Eng. Data* **2021**, *66*, 11−37.

(4) Kaşgöz, H.; Durmus, A. Dye removal by a novel hydrogel-clay nanocomposite with enhanced swelling properties. *Polym. Adv. Technol.* **2008**, *19*, 838−845.

(5) Crini, G. Non-conventional low-cost adsorbents for dye removal: A review. *Bioresour. Technol.* **2006**, *97*, 1061−1085.

(6) Pathania, D.; Gupta, D.; Al-Muhtaseb, A. a.H.; Sharma, G.; Kumar, A.; Naushad, M.; Ahamad, T.; Alshehri, S. M. Photocatalytic degradation of highly toxic dyes using chitosan-g-poly (acrylamide)/ZnS in presence of solar irradiation. *J. Photochem. Photobiol., A* **2016**, *329*, 61−68.

(7) Kokabian, B.; Bonakdarpour, B.; Fazel, S. The effect of salt on the performance and characteristics of a combined anaerobic-aerobic biological process for the treatment of synthetic wastewaters containing Reactive Black 5. *Chem. Eng. J.* **2013**, *221*, 363−372.

(8) Lau, Y.-Y.; Wong, Y.-S.; Teng, T.-T.; Morad, N.; Rafatullah, M.; Ong, S.-A. Coagulation-flocculation of azo dye Acid Orange 7 with green refined laterite soil. *Chem. Eng. J.* **2014**, *246*, 383−390.

(9) Luo, P.; Zhao, Y.; Zhang, B.; Liu, J.; Yang, Y.; Liu, J. Study on the adsorption of Neutral Red from aqueous solution onto halloysite nanotubes. *Water Res.* **2010**, *44*, 1489−1497.

(10) Ipek, I.; Kabay, N.; Yüksel, M. Separation of bisphenol A and phenol from water by polymer adsorbents: Equilibrium and kinetics studies. *J. Water Proc. Eng.* **2017**, *16*, 206−211.

https://doi.org/10.1021/acsomega.2c04904
ACS Omega 2022, 7, 41246−41255

(11) Batmaz, R.; Mohammed, N.; Zaman, M.; Minhas, G.; Berry, R. M.; Tam, K. C. Cellulose nanocrystals as promising adsorbents for the removal of cationic dyes. *Cellulose* **2014**, *21*, 1655−1665.
(12) Zhou, C.; Wu, Q.; Lei, T.; Negulescu, J. I. Adsorption kinetic and equilibrium studies for methylene blue dye by partially hydrolyzed polyacrylamide/cellulose nanocrystal nanocomposite hydrogels. *Chem. Eng. J.* **2014**, *251*, 17−24.
(13) Obeid, L.; El Kolli, N.; Dali, N.; Talbot, D.; Abramson, S.; Welschbillig, M.; Cabuil, V.; Bée, A. Adsorption of a cationic surfactant by a magsorbent based on magnetic alginate beads. *J. Colloid Interface Sci.* **2014**, *432*, 182−189.
(14) Firdaus, R. M.; Rosli, N. I. M.; Ghanbaja, J.; Vigolo, B.; Mohamed, A. R. Enhanced adsorption of methylene blue on chemically modified graphene nanoplatelets thanks to favorable interactions. *J. Nanopart. Res.* **2019**, *21*, 257.
(15) Dodero, A.; Pianella, L.; Vicini, S.; Alloisio, M.; Ottonelli, M.; Castellano, M. Alginate-based hydrogels prepared via ionic gelation: An experimental design approach to predict the crosslinking degree. *Eur. Polym. J.* **2019**, *118*, 586−594.
(16) Benhouria, A.; Islam, M. A.; Zaghouane-Boudiaf, H.; Boutahala, M.; Hameed, B. H. Calcium alginate−bentonite−activated carbon composite beads as highly effective adsorbent for methylene blue. *Chem. Eng. J.* **2015**, *270*, 621−630.
(17) Guo, R.; Jiao, T.; Li, R.; Chen, Y.; Guo, W.; Zhang, L.; Zhou, J.; Zhang, Q.; Peng, Q. Sandwiched Fe3O4/Carboxylate Graphene Oxide Nanostructures Constructed by Layer-by-Layer Assembly for Highly Efficient and Magnetically Recyclable Dye Removal. *ACS Sustainable Chem. Eng.* **2017**, *6*, 1279−1288.
(18) Zhao, H.; Jiao, T.; Zhang, L.; Zhou, J.; Zhang, Q.; Peng, Q.; Yan, X. Preparation and adsorption capacity evaluation of graphene oxide-chitosan composite hydrogels. *Sci. China Mater.* **2015**, *58*, 811−818.
(19) Li, N.; Yang, B.; Xu, L.; Xu, G.; Sun, W.; Yu, S. Simple synthesis of Cu2O/Na-bentonite composites and their excellent photocatalytic properties in treating methyl orange solution. *Ceram. Int.* **2016**, *42*, 5979−5984.
(20) Marco-Brown, J. L.; Guz, L.; Olivelli, M. S.; Schampera, B.; Torres Sánchez, R. M.; Curutchet, G.; Candal, R. New insights on crystal violet dye adsorption on montmorillonite: Kinetics and surface complexes studies. *Chem. Eng. J.* **2018**, *333*, 495−504.
(21) Liang, B.; Zhao, H.; Zhang, Q.; Fan, Y.; Yue, Y.; Yin, P.; Guo, L. Ca2+ Enhanced Nacre-Inspired Montmorillonite-Alginate Film with Superior Mechanical, Transparent, Fire Retardancy, and Shape Memory Properties. *ACS Appl. Mater. Interfaces* **2016**, *8*, 28816−28823.
(22) Eren, E. Adsorption Performance and Mechanism in Binding of Azo Dye by Raw Bentonite. *Clean: Soil, Air, Water* **2010**, *38*, 758−763.
(23) Errais, E.; Duplay, J.; Darragi, F.; M'Rabet, I.; Aubert, A.; Huber, F.; Morvan, G. Efficient anionic dye adsorption on natural untreated clay: Kinetic study and thermodynamic parameters. *Desalination* **2011**, *275*, 74−81.
(24) Han, H.; Rafiq, M. K.; Zhou, T.; Xu, R.; Mašek, O.; Li, X. A critical review of clay-based composites with enhanced adsorption performance for metal and organic pollutants. *J. Hazard. Mater.* **2019**, *369*, 780−796.
(25) Oussalah, A.; Boukerroui, A. Alginate-bentonite beads for efficient adsorption of methylene blue dye. *Euro-Mediterr. J. Environ. Integr.* **2020**, *5*, 31.
(26) Dai, H.; Huang, Y.; Huang, H. Eco-friendly polyvinyl alcohol/carboxymethyl cellulose hydrogels reinforced with graphene oxide and bentonite for enhanced adsorption of methylene blue. *Carbohydr. Polym.* **2018**, *185*, 1−11.
(27) Su, T.; Wu, L.; Pan, X.; Zhang, C.; Shi, M.; Gao, R.; Qi, X.; Dong, W. Pullulan-derived nanocomposite hydrogels for wastewater remediation: Synthesis and characterization. *J. Colloid Interface Sci.* **2019**, *542*, 253−262.
(28) Cheng, R.; Kang, M.; Zhuang, S.; Shi, L.; Zheng, X.; Wang, J. Adsorption of Sr(II) from water by mercerized bacterial cellulose membrane modified with EDTA. *J. Hazard. Mater.* **2019**, *364*, 645−653.
(29) Belhouchat, N.; Zaghouane-Boudiaf, H.; Viseras, C. Removal of anionic and cationic dyes from aqueous solution with activated organo-bentonite/sodium alginate encapsulated beads. *Appl. Clay Sci.* **2017**, *135*, 9−15.
(30) Meng, B.; Guo, Q.; Men, X.; Ren, S.; Jin, W.; Shen, B. Preparation of modified bentonite by polyhedral oligomeric silsesquioxane and sodium dodecyl sulfate in aqueous phase and its adsorption property. *Mater. Lett.* **2019**, *253*, 71−73.
(31) Saleh, T. A. The influence of treatment temperature on the acidity of MWCNT oxidized by HNO3 or a mixture of HNO3/H2SO4. *Appl. Surf. Sci.* **2011**, *257*, 7746−7751.
(32) Chen, B.; Li, Y.; Li, M.; Cui, M.; Xu, W.; Li, L.; Sun, Y.; Wang, M.; Zhang, Y.; Chen, K. Rapid adsorption of tetracycline in aqueous solution by using MOF-525/graphene oxide composite. *Microporous Mesoporous Mater* **2021**, *328*, 11457.
(33) Chen, L.; Li, Y.; Du, Q.; Wang, Z.; Xia, Y.; Yedinak, E.; Lou, J.; Ci, L. High performance agar/graphene oxide composite aerogel for methylene blue removal. *Carbohydr. Polym.* **2017**, *155*, 345−353.
(34) Xia, J.; Gao, Y.; Yu, G. Tetracycline removal from aqueous solution using zirconium-based metal-organic frameworks (Zr-MOFs) with different pore size and topology: Adsorption isotherm, kinetic and mechanism studies. *J. Colloid Interface Sci.* **2021**, *590*, 495−505.
(35) Yao, K.; Huang, S.; Tang, H.; Xu, Y.; Buntkowsky, G.; Berglund, L. A.; Zhou, Q. Bioinspired Interface Engineering for Moisture Resistance in Nacre-Mimetic Cellulose Nanofibrils/Clay Nanocomposites. *ACS Appl. Mater. Interfaces* **2017**, *9*, 20169−20178.
(36) Saleh, T. A. Carbon nanotube-incorporated alumina as a support for MoNi catalysts for the efficient hydrodesulfurization of thiophenes. *Chem. Eng. J.* **2021**, *404*, 126987.
(37) Wang, W.; Zheng, B.; Deng, Z.; Feng, Z.; Fu, L. Kinetics and equilibriums for adsorption of poly(vinyl alcohol) from aqueous solution onto natural bentonite. *Chem. Eng. J.* **2013**, *214*, 343−354.
(38) Burwell, R. L.*Manual of Symbols and Terminology for Physicochemical Quantities and Units—Appendix II Heterogeneous Catalysis*; Elsevier, 1977, pp 351−392.
(39) Macedo, S.; da Costa Júnior, N. B.; Almeida, L. E.; Vieira, E. F.; Cestari, A. R.; Gimenez, F.; Villarreal Carreño, N. L.; Barreto, L. S. Kinetic and calorimetric study of the adsorption of dyes on mesoporous activated carbon prepared from coconut coir dust. *J. Colloid Interface Sci.* **2006**, *298*, 515−522.
(40) Usman, M.; Ahmed, A.; Yu, B.; Wang, S.; Shen, Y.; Cong, H. Simultaneous adsorption of heavy metals and organic dyes by beta-Cyclodextrin-Chitosan based cross-linked adsorbent. *Carbohydr. Polym.* **2021**, *255*, 117486.
(41) Lin, S.; Song, Z.; Che, G.; Ren, A.; Li, P.; Liu, C.; Zhang, J. Adsorption behavior of metal−organic frameworks for methylene blue from aqueous solution. *Microporous Mesoporous Mater.* **2014**, *193*, 27−34.
(42) Chang, J.; Ma, J.; Ma, Q.; Zhang, D.; Qiao, N.; Hu, M.; Ma, H. Adsorption of methylene blue onto Fe3O4/activated montmorillonite nanocomposite. *Appl. Clay Sci.* **2016**, *119*, 132−140.
(43) Hameed, B. H.; Ahmad, A. A. Batch adsorption of methylene blue from aqueous solution by garlic peel, an agricultural waste biomass. *J. Hazard. Mater.* **2009**, *164*, 870−875.
(44) Ncibi, M. C.; Mahjoub, B.; Seffen, M. Kinetic and equilibrium studies of methylene blue biosorption by Posidonia oceanica (L.) fibres. *J. Hazard. Mater.* **2007**, *139*, 280−285.
(45) Zaghouane-Boudiaf, H.; Boutahala, M. Kinetic analysis of 2,4,5-trichlorophenol adsorption onto acid-activated montmorillonite from aqueous solution. *Int. J. Miner. Process.* **2011**, *100*, 72−78.
(46) Gupta, V. K.; Jain, R.; Siddiqui, M. N.; Saleh, T. A.; Agarwal, S.; Malati, S.; Pathak, D. Equilibrium and Thermodynamic Studies on the Adsorption of the Dye Rhodamine-B onto Mustard Cake and Activated Carbon. *J. Chem. Eng. Data* **2010**, *55*, 5225−5229.
(47) Yu, K. L.; Lee, X. J.; Ong, H. C.; Chen, W.-H.; Chang, J.-S.; Lin, C.-S.; Show, P. L.; Ling, T. C. Adsorptive removal of cationic methylene blue and anionic Congo red dyes using wet-torrefied

https://doi.org/10.1021/acsomega.2c04904
ACS Omega 2022, 7, 41246−41255

microalgal biochar: Equilibrium, kinetic and mechanism modeling. *Environ. Pollut.* **2021**, *272*, 115986.
(48) Zhao, X.; Wang, X.; Lou, T. Preparation of fibrous chitosan/sodium alginate composite foams for the adsorption of cationic and anionic dyes. *J. Hazard. Mater.* **2021**, *403*, 124054.
(49) Li, L.; Li, Y.; Yang, K.; Li, M.; Luan, X.; Sun, Y.; Wang, H.; Sun, Q.; Tang, K.; Zheng, H.; Cui, M.; Xu, W. Adsorption of methylene blue by Nicandra physaloides(L.) Gaertn seed gum/graphene oxide aerogel. *Environ. Technol.* **2022**, *43*, 2342−2351.
(50) Zhang, Z.; Li, Y.; Du, Q.; Li, Q. Adsorption of congo red from aqueous solutions by porous soybean curd xerogels. *Pol. J. Chem. Technol.* **2018**, *20*, 95−102.
(51) Ho, Y. S.; McKay, G. A comparison of chemisorption kinetic models applied to pollutant removal on various sorbents. *Process Saf. Environ. Prot.* **1998**, *76*, 332−340.
(52) Li, Y.; Du, Q.; Liu, T.; Qi, Y.; Zhang, P.; Wang, Z.; Xia, Y. Preparation of activated carbon from Enteromorpha prolifera and its use on cationic red X-GRL removal. *Appl. Surf. Sci.* **2011**, *257*, 10621−10627.
(53) Li, M.; Li, Y.; Zhang, X.; Zheng, H.; Zhang, A.; Chen, T.; Liu, W.; Yu, Y.; Liu, J.; Du, Q.; Wang, D.; Xia, Y. One-step generation of S and N co-doped reduced graphene oxide for high-efficiency adsorption towards methylene blue. *RSC Adv.* **2020**, *10*, 37757−37765.
(54) Li, W.; Zuo, P.; Xu, D.; Xu, Y.; Wang, K.; Bai, Y.; Ma, H. Tunable adsorption properties of bentonite/carboxymethyl cellulose-g-poly(2-(dimethylamino) ethyl methacrylate) composites toward anionic dyes. *Chem. Eng. Res. Des.* **2017**, *124*, 260−270.
(55) Zhang, P.; Ouyang, S.; Li, P.; Huang, Y.; Frost, R. L. Enhanced removal of ionic dyes by hierarchical organic three-dimensional layered double hydroxide prepared via soft-template synthesis with mechanism study. *Chem. Eng. J.* **2019**, *360*, 1137−1149.
(56) Li, Y.; Gao, C.; Jiao, J.; Cui, J.; Li, Z.; Song, Q. Selective Adsorption of Metal-Organic Framework toward Methylene Blue: Behavior and Mechanism. *ACS Omega* **2021**, *6*, 33961−33968.
(57) Makhado, E.; Pandey, S.; Ramontja, J. Microwave assisted synthesis of xanthan gum-cl-poly (acrylic acid) based-reduced graphene oxide hydrogel composite for adsorption of methylene blue and methyl violet from aqueous solution. *Int. J. Biol. Macromol.* **2018**, *119*, 255−269.
(58) Gomri, F.; Boutahala, M.; Zaghouane-Boudiaf, H.; Korili, S. A.; Gil, A. Removal of acid blue 80 from aqueous solutions by adsorption on chemical modified bentonites. *Desalin. Water Treat.* **2016**, *57*, 26240−26249.
(59) Şahin, Ö.; Kaya, M.; Saka, C. Plasma-surface modification on bentonite clay to improve the performance of adsorption of methylene blue. *Appl. Clay Sci.* **2015**, *116−117*, 46−53.
(60) Liu, C.; Omer, A. M.; Ouyang, X. K. Adsorptive removal of cationic methylene blue dye using carboxymethyl cellulose/k-carrageenan/activated montmorillonite composite beads: Isotherm and kinetic studies. *Int. J. Biol. Macromol.* **2018**, *106*, 823−833.
(61) Li, H.; Zhang, D.; Han, X.; Xing, B. Adsorption of antibiotic ciprofloxacin on carbon nanotubes: pH dependence and thermodynamics. *Chemosphere* **2014**, *95*, 150−155.
(62) Tang, S.; Xia, D.; Yao, Y.; Chen, T.; Sun, J.; Yin, Y.; Shen, W.; Peng, Y. Dye adsorption by self-recoverable, adjustable amphiphilic graphene aerogel. *J. Colloid Interface Sci.* **2019**, *554*, 682−691.
(63) Ravi, L.; Pandey, L. M. Enhanced adsorption capacity of designed bentonite and alginate beads for the effective removal of methylene blue. *Appl. Clay Sci.* **2019**, *169*, 102−111.
(64) Sun, Y.; Li, Y.; Chen, B.; Cui, M.; Xu, W.; Li, L.; Wang, M.; Zhang, Y.; Chen, K.; Du, Q.; Wang, Y.; Pi, X. High-Efficiency Adsorption Performance of Cobalt Alginate/ Graphene Oxide Aerogel Prepared by Green Method for Methylene Blue. *Chemistryselect* **2022**, *7*, No. e202201216.

https://doi.org/10.1021/acsomega.2c04904
ACS Omega 2022, 7, 41246−41255